Climate Dynamics (2024) 62:9361–9375
https://doi.org/10.1007/s00382-024-07399-5

ORIGINAL ARTICLE

Predictability of the early summer surface air temperature over Western South Asia

Irfan Ur Rashid[1] · Muhammad Adnan Abid[2,3] · Marisol Osman[4,5] · Fred Kucharski[3] · Moetasim Ashfaq[6] · Antje Weisheimer[2,7] · Mansour Almazroui[8,9] · José Abraham Torres-Alavez[10] · Muhammad Afzaal[1]

Received: 11 December 2023 / Accepted: 7 August 2024 / Published online: 22 August 2024

Abstract
Variability of the Surface Air Temperature (SAT) over the Western South Asia (WSA) region leads to frequent heatwaves during the early summer (May-June) season. The present study uses the European Centre for Medium-Range Weather Forecast's fifth-generation seasonal prediction system, SEAS5, from 1981 to 2022 based on April initial conditions (1-month lead) to assess the SAT predictability during early summer season. The goal is to evaluate the SEAS5's ability to predict the El Niño-Southern Oscillation (ENSO) related interannual variability and predictability of the SAT over WSA, which is mediated through upper-level (200-hPa) geopotential height anomalies. This teleconnection leads to anomalously warm surface conditions over the region during the negative ENSO phase, as observed in the reanalysis and SEAS5. We evaluate SEAS5 prediction skill against two observations and three reanalyses datasets. The SEAS5 SAT prediction skill is higher with high spatial resolution observations and reanalysis datasets compared to the ones with low-resolution. Overall, SEAS5 shows reasonable skill in predicting SAT and its variability over the WSA region. Moreover, the predictability of SAT during La Niña is comparable to El Niño years over the WSA region.

Keywords Predictability · ECMWF-SEAS5 · ENSO · Temperature variability · WSA · La Niña

1 Introduction

Understanding the predictability of Surface Air Temperature. (SAT) and its sources on sub-seasonal to seasonal (S2S) timescales is useful for planning vis-à-vis the regional socio-economic sectors. Many regions have experienced unprecedented heatwaves in recent decades, including Chicago, USA in 1995, Europe in 2003 and 2019, Russia in 2010, Australia in 2019, and South Asia in 2010, 2015, and 2019 (Perkins 2015; Campbell et al. 2018; Vogel et al.

✉ Muhammad Adnan Abid
adnan.abid@physics.ox.ac.uk

1 Research and Development Division, Pakistan Meteorological Department, Islamabad, Pakistan

2 Atmospheric, Oceanic and Planetary Physics (AOPP), Department of Physics, University of Oxford, Oxford, UK

3 Earth System Physics, Abdus Salam International Centre for Theoretical Physics (ICTP), Trieste, Italy

4 Karlsruhe Institute of Technology, Karlsruhe, Germany

5 Universidad de Buenos Aires, Facultad de Ciencias Exactas y Naturales, Departamento de Ciencias de la Atmósfera y los Océanos, CONICET – Universidad de Buenos Aires, Centro de Investigaciones del Mar y la Atmósfera (CIMA), CNRS – IRD – CONICET – UBA, Instituto Franco-Argentino para el Estudio del Clima y sus Impactos (IRL 3351 IFAECI), Buenos Aires, Argentina

6 Computational Sciences and Engineering Division, Oak Ridge National Laboratory, Oak Ridge, TN, USA

7 European Centre for Medium-Range Weather Forecasts (ECMWF), Reading, UK

8 Centre of Excellence for Climate Change Research (CECCR), Department of Meteorology, King Abdulaziz University, Jeddah, Saudi Arabia

9 Climatic Research Unit, School of Environmental Sciences, University of East Anglia, Norwich, UK

10 Danish Meteorological Institute, Copenhagen, Denmark

2019). In Spring 2022, a 4–5 °C temperature anomaly has been noted over north-west South Asia (Nath et al. 2024). It shattered a 122-year-old temperature record, affecting more than 1.5 billion people in the region. The frequency and intensity of the hot extremes have increased alarmingly over Western South Asia (WSA) and are projected to increase by the end of the 21st century (Almazroui et al. 2020). Consequently, densely populated regions, including Pakistan, Iran, Afghanistan, northwest India, and some Central Asian states, are likely to be affected by the extreme temperatures. According to some estimates, by 2030, the warm events may contribute significantly (about 4–5%) to the regional Gross Domestic Product (GDP) losses (Price and Farhan 2022; Zachariah et al. 2022). In general, the WSA climate is classified as a semi-arid to arid climate, including the western half of the HinduKush Himalaya (HKH) mountains ranges with many glaciers (Fig. 1a, highlighted as box), which are the freshwater and hydropower energy sources for the downstream regions (Chaturvedi et al. 2014; Pritchard 2019). Any anomalous conditions in the WSA temperature may escalate energy demands and negatively impact agricultural resources, such as wheat crops. The rising temperature may also harm regional water availability due to river flooding caused by the rampant melting of glaciers (Mannig et al. 2018; Zhongming et al. 2021). Therefore, predicting anomalous temperature conditions by dynamical seasonal prediction systems on S2S timescales is challenging, which may impede building a climate-resilient society for billions of people in the region.

Based on Coupled Global Climate Models (CGCMs), dynamical seasonal prediction systems are valuable tools for climate forecasting on S2S timescales (Kang et al. 2004; Kang and Shukla 2006; Wang et al. 2009; Delsole et al. 2011; Kirtman et al. 2014; Vitart and Robertson 2018; Almazroui et al. 2022; Osman et al. 2023). El Niño-Southern Oscillation (ENSO) teleconnections are considered a prominent source of variability and predictability on S2S timescales (Trenberth et al. 2002; Palmer et al. 2004; Kucharski et al. 2010; Kang and Lee 2019; McPhaden et al. 2020; Taschetto et al. 2020) and have a widespread effect on the climate

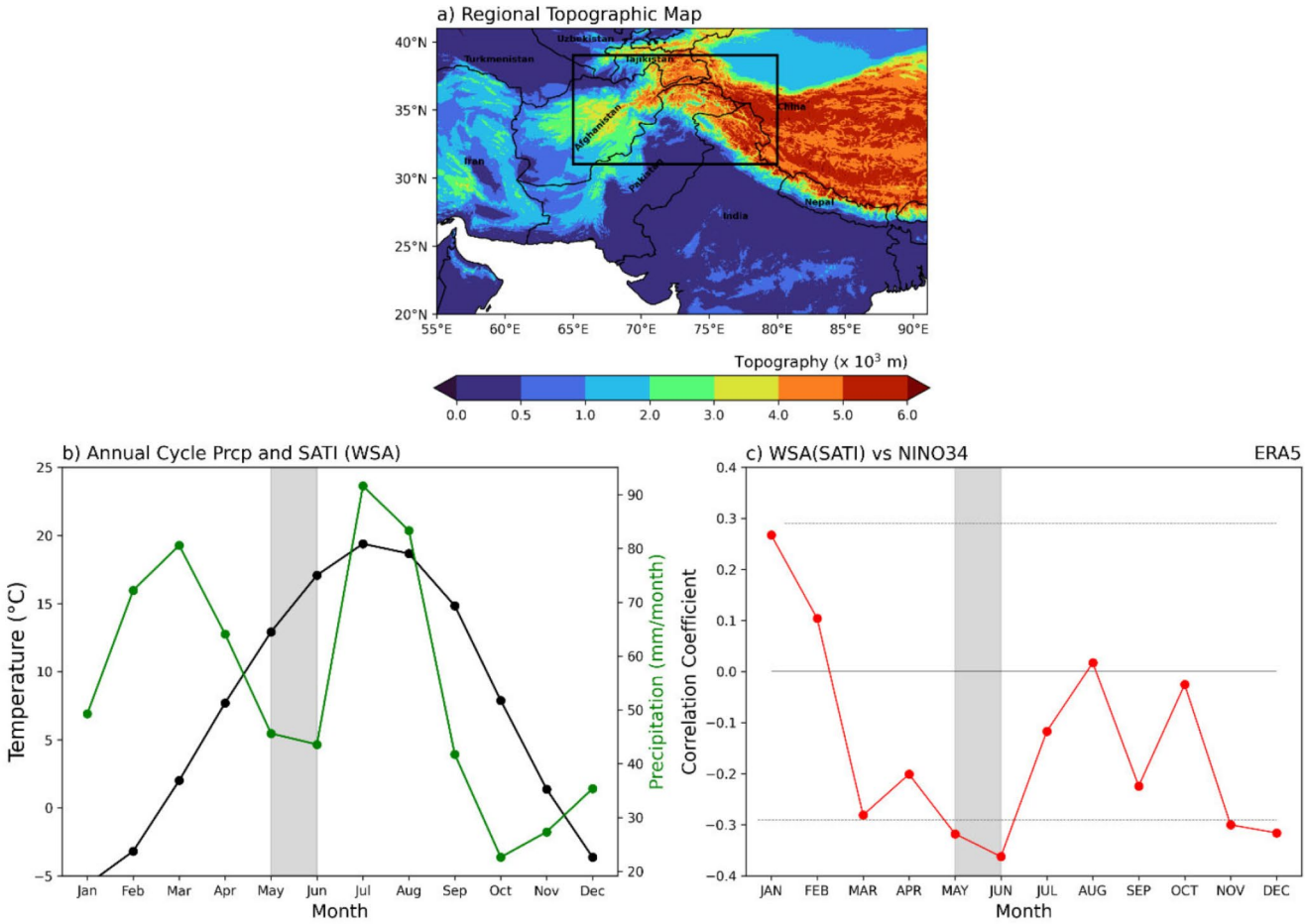

Fig. 1 (**a**) Regional topographic map for South Asia (Unit: m), where black rectangular box highlights the Western South Asian (WSA) region, as study region; (**b**) Annual cycle of SAT Index (SATI) area-averaged over the WSA [65°E–80°E; 31°N -39°N] region (black line, Unit: °C) and precipitation (green line, Unit: mm/month) over WSA; (**c**) Monthly relationship between Niño3.4 and SATI over WSA region shown in Fig. 1a

extremes (e.g., flooding, heatwaves) globally (Attada et al. 2018; Joshi et al. 2020; Hoell et al. 2021). Models are mostly skilful in the extended range ENSO predictions up to several months (Almazroui et al. 2022). Several earlier studies have underlined the role of ENSO in the boreal summer (JJA) season SAT variability across the Indian region (Kothawale et al. 2010; Chowdary et al. 2014; Thirumalai et al. 2017; Zheng et al. 2017; Ehsan 2020; Joshi et al. 2020), but limited information is available for SAT variability and predictability, particularly during the early summer (May-June) season over the WSA region.

SAT over South Asia peaks during the early summer (i.e., the pre-monsoon season) (Chelani and Rao 2013; Zhou et al. 2019; Ehsan 2020). The maximum of this peak occurs in the eastern half of South Asia, where monsoon begins in early June, propagates north-westward, and onsets in the first week of July over the WSA region (Latif and Syed 2016; Ashfaq et al. 2021). Therefore, for WSA, the pre-monsoon (early summer) period is from May to June, which plays a crucial role in shaping the atmospheric conditions and the progression of the monsoon towards the WSA region (Lau et al. 2006; Saeed et al. 2011; Rai et al. 2015). A significant upper-level anticyclonic circulation (also known as South Asian High; SAH) helps to steer the monsoon winds into Pakistan and northwestern India (Liu et al. 2013; Wei and Yang 2021). The upper-level (200-hPa) positive geopotential height anomalies modulate the interannual variability of the SAT over the WSA region through middle tropospheric warming, low cloud cover, and increased surface shortwave radiation that favours warming surface conditions over the region (Saeed et al. 2013; Rashid et al. 2022).

During early summer, ENSO, in its negative phase, reinforces upper-level positive geopotential height anomalies over the WSA region by strengthening the upper-level divergence over the western Pacific. This teleconnection enhances the sinking motion and favours clear- sky conditions leading to extremely high surface temperatures over the WSA region, including Pakistan in the cold ENSO phase. The opposite happens in the warm ENSO phase (Rashid et al. 2022). However, how well dynamical seasonal prediction systems predict the SAT over WSA in the early summer has yet to be known, which is the focus of the current study. The rest of the manuscript is arranged as follows: The data and methodology are discussed in Sect. 2, the teleconnections and predictability results are shown in Sect. 3, and Sect. 4 presents the summary and conclusions.

2 Datasets and methodology

2.1 Observational and reanalysis datasets

Monthly reanalysis SAT, Sea Surface Temperatures (SSTs), and 200-hPa geopotential height datasets used in this study were obtained from the fifth generation European Re-Analysis (ERA5) at 0.25°×0.25° horizontal grid spacing for the period 1981–2022 (Copernicus Climate Change Service (C3S) 2017; Hersbach et al. 2020). The complex topography of the WSA and sparsity of ground observations contribute to the uncertainties in the observational and reanalysis datasets over the region (Saini and Attada 2023). To understand the uncertainties in seasonal forecast quality and skill when comparing to different datasets, we utilized the monthly mean SATs from the National Centre for Environmental Prediction (NCEP)/National Centre for Atmospheric Research (NCAR) at a spatial resolution of 2.5° × 2.5° longitude and latitude (Kalnay et al. 1996), Climatic Research Unit (CRU) at a spatial resolution of 0.5° × 0.5° longitude and latitude (Harris et al. 2020), Modern-Era Retrospective Analysis for Research and Applications, Version 2 (MERRA-2) at a spatial resolution of 0.5° x 0.625° latitude and longitude (Gelaro et al. 2017) and Climate Prediction Centre (CPC) at a spatial resolution of 0.5° × 0.5° longitude and latitude in addition to ERA5. For details, see Table S1. The topography dataset was obtained from the 2-minute Gridded Global Relief Data (ETOPO2v2) at a spatial resolution of 2 arc-minutes (NOAA 2006).

The ERA5 SAT anomalies over the WSA [65°E–80°E; 31°N–39°N] region are comparable to the observational SAT from CRU (Correlation Coefficient; CC = 0.92) and CPC (CC = 0.95). Also, the CC between CPC and CRU is 0.94, while for NCEP and MERRA-2 is 0.78. This correspondence between ERA5 and observations as well as reanalysis has also been reported earlier, suggesting that ERA5 performs better than the other reanalysis and is also comparable with the in-situ observations over the region (Arshad et al. 2021; Iqbal et al. 2022; Rashid et al. 2022).

2.2 ECMWF model hindcast dataset

We have used the European Centre for Medium-Range Weather Forecasts (ECMWF) fifth-generation seasonal prediction system SEAS5 reforecast dataset (Johnson et al., 2019) to analyse early summer season (May-June; MJ) SAT prediction skill over WSA at lead-1 (April initial condition). A hindcast dataset of 25 ensemble members, initialized with perturbed initial states, is available for each year from 1981 to 2016. In addition, the 25-ensemble member forecasts from 2017 to 2022 are also included to extend the analysis to the period 1981 to 2022. The model, reanalysis, and

observations are re-gridded to a common 1°×1° horizontal grid. All datasets, including observations, reanalysis, and each ensemble member of SEAS5, are detrended linearly. The anomalies are estimated with reference to the 1981 to 2022 period.

During the early summer season, the prediction skill of SEAS5 weighted area-averaged SST anomalies over the ENSO region (Niño3.4 [190°E–240°E; 5°S–5°N] is 0.9, while for May (Lead-1) and June (Lead-2) months, it is 0.93 and 0.86, respectively, which demonstrates that SEAS5 is skillful in ENSO predictions for this season.

2.3 Methods

Empirical Orthogonal Function (EOF) analysis is used to analyse the interannual variability of the early summer SATs over WSA. Linear regressions are performed to investigate ENSO teleconnections, defined as the covariance of the standardized anomaly index with the required global anomaly field (Molteni et al. 2015; Abid et al. 2020; Rashid et al. 2022). The model (SEAS5) EOF is analysed after concatenating all ensemble members (**m**) over all years (**n**), where total concatenated sample size is **(m x n)**. Therefore, for 25 ensemble members over 42 years, the sample size is (42×25 = 1050). A weighted area-averaged (using the cosine weighting latitude function) SAT index over WSA (referred to as SATI) domain [65°E–80°E; 31°N–39°N] is defined for the period 1981–2022.

The Probability Distribution Function (PDF) is evaluated for concatenated SEAS5 SAT anomalies over the WSA region during the early summer season, using the Kernel Density Estimation (KDE), where 25 ensemble members are available for 42 years (25×42 = 1050). Each ensemble member's Niño3.4 SST anomaly index was estimated. The El Niño and La Niña years of early summer seasonal SAT anomalies for each ensemble member were defined based on the Niño3.4 ($\geq \pm 0.5$ °C) index. Of 1050 SAT years, 227 are binned for El Niño, while 215 are the La Niña years. Similarly, the model SAT seasonal mean anomalies are binned into El Niño and La Niña years while constraining it to the ERA5 Niño3.4 index. In this case, early summer seasonal SAT anomalies for El Niño and La Niña years are 225 and 250 years (sample size), respectively.

A student two-tailed t-test is used to test the statistical significance of the results (Wilks 2006). The t-value is calculated using the Eq. (1)

$$t = \frac{r * \sqrt{(n-2)}}{1 - \sqrt{(1-r^2)}} \tag{1}$$

Where '***r***' is the correlation coefficient of the two variables, quantifying the strength and direction of the linear relationship, and '***n***' is the degree of freedom. Our null hypothesis (H_0) states that there is no significant correlation between the two variables (uncorrelated), while the alternative hypothesis (H_1) suggests that there is a significant correlation.

Similarly, for composite significance, the t-values are calculated using Eq. (2)

$$t = \frac{\bar{x} - \mu_0}{s/\sqrt{n}} \tag{2}$$

Where '$\bar{x}$' is the composite mean, μ_0 is the total sample mean, 's' is the standard deviation, and '***n***' is the degree of freedom. The null hypothesis is that $\bar{x}$ is equal to μ_0.

The statistical significance of the result is attributed to the values when a relationship is identified between the two variables, resulting in the null hypothesis being rejected at the 5% significance level (or 95% confidence level). For the composite analysis, the null hypothesis is rejected when the composite mean differs from the total sample mean at the 10% significance level (or 90% confidence level).

2.4 Predictability measures

Potential Predictability (PP) measures the potential skill of a model in predicting weather and climate systems over specific regions (Kang and Shukla 2006; Younas and Tang 2013; Kumar et al. 2014). It primarily depends on the signal and the noise variances (Scaife and Smith 2018), where signal variance is defined as the variances of the ensemble mean anomalies, and noise variance is the variances of the deviation of each member from the ensemble mean (Kang and Shukla 2006; Eade et al. 2014; Abid et al. 2015; Hardiman et al. 2022). PP is estimated as the square root of the signal variance to the total (signal and noise) variance (Eade et al. 2014; Abid et al. 2016; Osman and Vera 2017; Kucharski and Abid 2017; Hardiman et al. 2022). Moreover, the actual skill assesses how well the climate system evolves in the model compared to the observations. It is calculated as the grid-to-grid correlation between the observations/reanalysis and the model ensemble mean anomalies. The model's behaviour is considered overconfident when PP is higher than the actual skill and under-confident in the opposite case (Scaife and Smith 2018; Abid et al. 2023).

To analyse the PP of the temperature during the ENSO phases (i.e., El Niño and La Niña years), the signal is defined as the mean of the square of each El Niño/La Niña year ensemble mean anomaly, and the noise is defined as the variance over the ensemble members for the particular ENSO (El Niño/La Niña) year. The anomaly for each El Niño/La Niña year is estimated as shown in Eq. (3) (Abid et al. 2018).

$$SAT'_{(ensoyear)_i} = SAT_{(ensoyear)_i} - \bar{SAT}_{1981-2022} \quad (3)$$

Here, (***i***) represents ENSO (El Niño/La Niña) year, while $\bar{SAT}$ is the climatological mean for the total period 1981–2022.

3 Results

3.1 Early summer SAT mean and variability over Western South Asia

The WSA region is characterized by its high mountainous terrain (Fig. 1a) where annual SAT variability reaches 1.62 °C, during the early summer season. This is larger than the SAT variability noted in the conventional boreal summer (June-July-August; JJA) season (1.18 °C) and the monsoonal (July-August-September, JAS) season (1.14 °C) over the WSA region (Ashfaq et al. 2023). Notably, in the annual cycle, the mean temperature peaks (black line) in the JJA season (Fig. 1b). Moreover, the monsoon onsets (green line; Fig. 1b) over the WSA region is on average in the first week of July consistent with earlier findings (Latif and Syed 2016; Ashfaq et al. 2021). We also analysed monthly contemporaneous ENSO teleconnections with SAT over the WSA region, where the relationship peaks during May and June months (statistically significant at 95% confidence level), as shown in Fig. 1c. Therefore, the early summer season (MJ) is characterized by hot and dry climate for WSA region, where hot conditions are likely to be experienced during negative ENSO phase (Rashid et al. 2022).

Figure 2 compares the ERA5 early summer SAT mean climatology and standard deviation (STD) with the model (SEAS5) dataset over WSA for the period 1981 to 2022. The mean SAT climatology distribution of the ERA5 (Fig. 2a) shows a north-to-south gradient, which is well represented in the seasonal re-forecast dataset (Fig. 2b). The high mountain terrain in northern South Asia leads to the contrasting temperature gradient from south to north where the temperature reaches its maximum (about 40 °C) in the south with maxima over the central to southern Pakistan, while it ranges to about 5 °C in the north in ERA5. This north-south temperature gradient is well represented in SEAS5 (Fig. 2a-b). Moreover, the interannual SAT variability is maximum in the north and northwest South Asian region that reaches 1.8 °C STD (Fig. 2c), which is well simulated in the SEAS5 (Fig. 2d). Note that the SEAS5 STD is estimated as the square root of the mean variance of the ensemble members.

We evaluated the model skill using different observations and reanalysis datasets to assess the data-based uncertainties (Fig. S1). For details of the observational and reanalysis dataset, see Table S1. Most of the datasets compare well

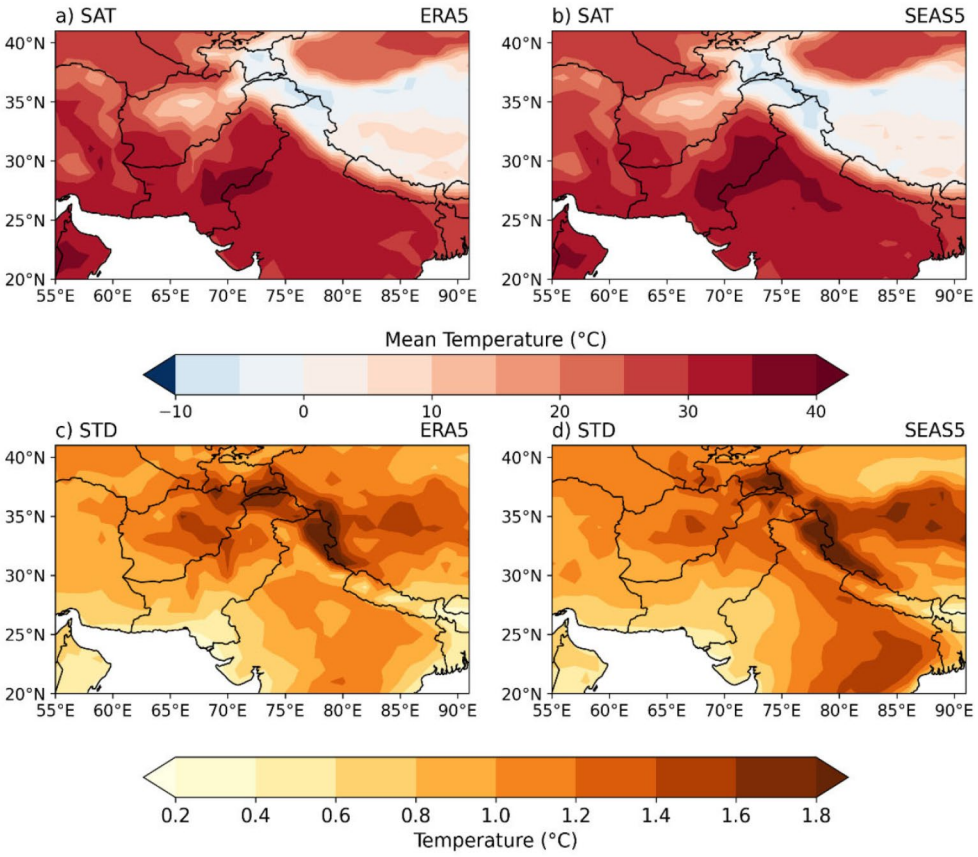

Fig. 2 **a-b**) Mean surface air temperature (SAT) of reanalysis (ERA5) and ECMWF-SEAS5 during early summer (May-June: MJ) season for the period 1981–2022; **c-d**) Same as of (**a-b**) but for the standard deviation (STD). Unit is (°C)

with ERA5 except for the NCEP over WSA (Fig. S2). The difference in NCEP can be related to its coarser horizontal spatial resolution than the other observations and ERA5. Also, the CRU dataset shows lower variability, which could be because of the lower density of the observational network in the region, particularly in the areas with complex terrain.

Furthermore, a cold temperature bias is noted between SEAS5 and ERA5 in the high topographical region of northern Pakistan and northwestern India. In contrast, a warm bias is noted over central parts of India and Pakistan (Fig. S3a). Similarly, the root-mean-square error (RMSE) displays a significant bias over the high mountainous region (WSA; Fig. S3b). Overall, SEAS5 shows a cold bias compared to most of the dataset, with the minimum noted against ERA5, except that of NCEP, where a warm bias is noted in SAT over the WSA region (Fig. S4).

The SAT spatiotemporal variability for ERA5 and SEAS5 over WSA is analysed using EOF analysis. The ERA5 leading first mode (EOF1) explains approximately 45% of the total variance (Fig. 3a), where SAT maxima appear over northern Pakistan, Afghanistan, and northwestern parts of India in the WSA region, consistent with Fig. 2(c). For the SEAS5 EOF analysis, we concatenated the 25 ensemble members, resulting in a 1050 sample size (42 × 25). The model (SEAS5) EOF1 represents the spatial distribution of SAT quite well (Fig. 3b), explaining 38% of the total variance. This pattern closely aligns with the ERA5 SAT variability pattern (Fig. 3a) and the SEAS5 interannual variability over the region (Fig. 2d). Figure 3c shows the temporal evolution of PC1 in ERA5 and SEAS5 with a CC of 0.53 (statistically significant at the 95% confidence level). The CC between the ERA5-based SAT index (SATI) and the corresponding PC1 is 0.99. Therefore, the rest of the analyses related to temperature variability over the WSA region are based on SATI (Fig. 3c).

3.2 Early summer SAT teleconnections in reanalysis and SEAS5 forecasting system

Early summer SAT teleconnections are analysed in the ERA5 and the SEAS5 prediction system because well-represented teleconnections may provide skilful S2S regional predictions (Kucharski et al. 2010; Abid et al. 2016; Ehsan et al. 2019; Taschetto et al. 2020). Figure 4(a-b) shows the scatter plot between SATI and Niño3.4 index for the ERA5 and SEAS5, respectively. The slope in ERA5 is -0.74 (°C/°C), while the SEAS5 slope is -0.44 (°C/°C), suggesting SAT over the WSA is slightly less sensitive to ENSO SST anomalies in SEAS5 compared to ERA5. Furthermore, a statistically significant (95% confidence level) negative CC = -0.42 is noted between the SATI over the WSA and Niño3.4 in ERA5. For SEAS5, we computed a scatter plot (grey dots) based on all ensemble members, where a weaker negative relationship (CC= -0.31) is noted between SATI and Niño34, which is almost half of the ensemble mean (CC= -0.60) shown in black circles. The weaker relationship is related to the large variability among the members.

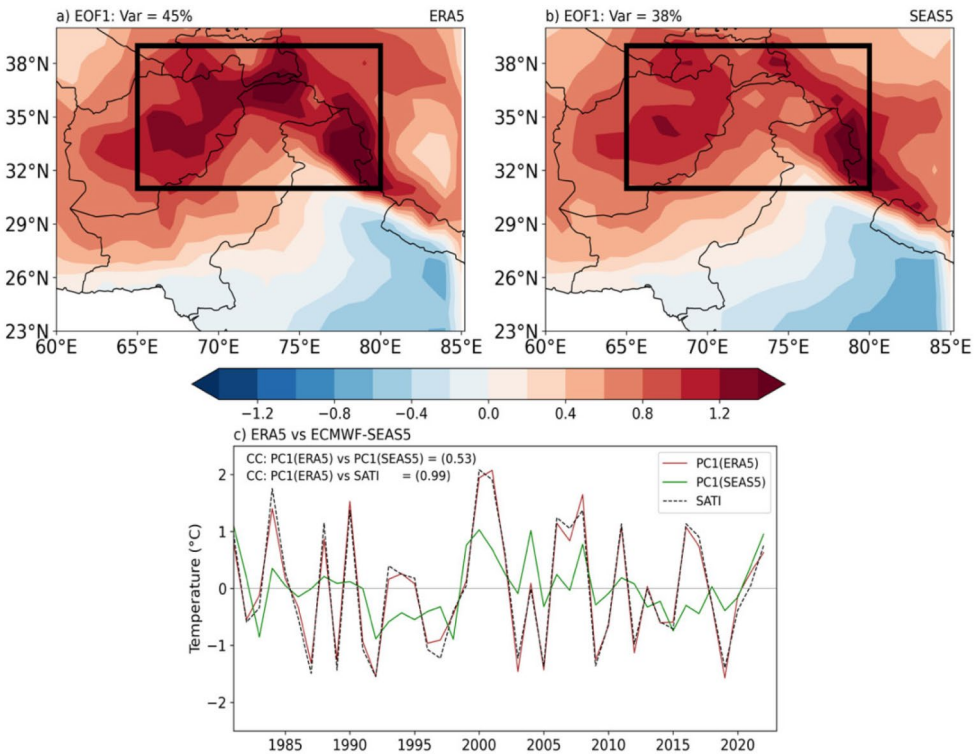

Fig. 3 **a-b**) Leading (First) mode of Empirical Orthogonal Function (EOF1) of the SAT during early summer season over the Western South Asia (WSA) region for the ERA5 and SEAS5 dataset respectively for the period 1981–2022; **c**) PC1 associated with leading (first) EOFs for ERA5 (red Line), SEAS5 (green line) and SAT Index (SATI, highlighted as box in Fig. 2a; black line) averaged over the WSA domain [65–80°E; 31°N -39°N]. Unit is (°C)

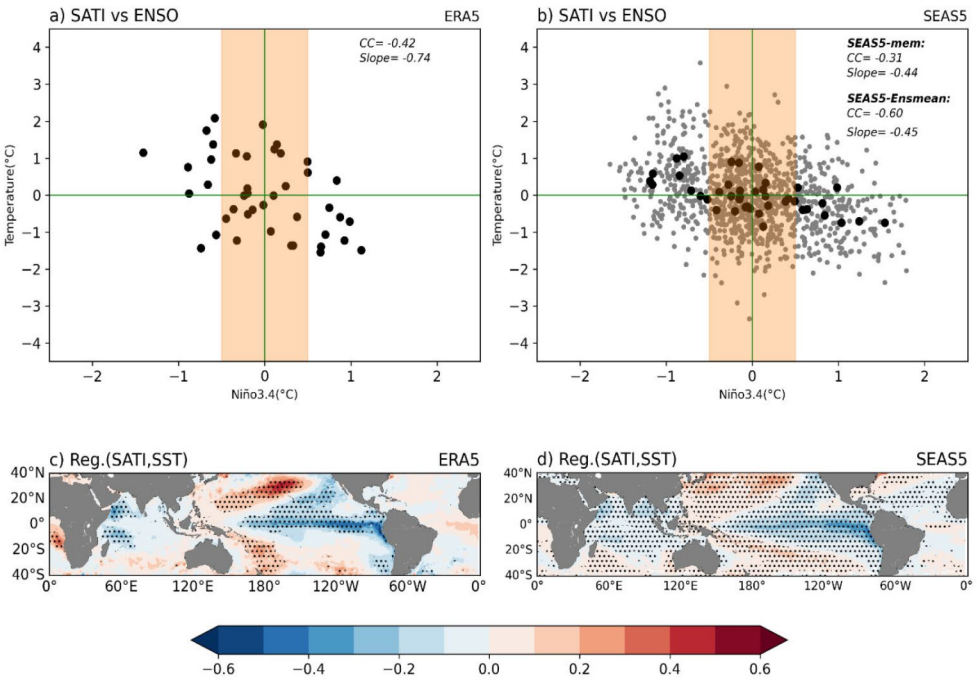

Fig. 4 **a-b**) Scatter Plot between the Niño3.4 (x-axis) and the SATI for ERA5 and SEAS5 respectively, during early summer season for the period 1981–2022. The ERA5 slope (CC) is -0.74 °C /°C (-0.42) and for SEAS5 based on ensemble mean is -0.45 °C /°C (-0.60). Shading in a-b) indicates the neutral ENSO phase; **c-d**) Regression maps of global SST onto the standardized SATI of WSA for ERA5 and ECMWF-SEAS5 respectively for the period 1981–2022. Unit is (°C). SEAS5 regression map is based on the mean of the 25-ensemble members. Stippling represents the statistical significance at 95% confidence level

The negative relationship shows anomalous warm SAT may occur over the WSA region during La Niña.

Moreover, the ERA5 regression of early summer SST onto the corresponding standardized SATI is shown in Fig. 4c, where negative SST anomalies appear in the central-eastern equatorial Pacific region (i.e., the ENSO region). Similarly, the SEAS5 regression is performed for each ensemble member. The mean regression of 25 members is shown in Fig. 4d, which is consistent with ERA5 (Fig. 4c). A significant SST anomaly also appears over the western Indian Ocean and tropical Atlantic region; however, in this study, we restrict our focus on ENSO forced predictability for the regional temperature. We noted ERA5 SAT-ENSO regression coefficient lies within the spread of the regression coefficients (regression coefficients are multiplied with − 1) of individual ensemble members but towards the upper end of ensemble distribution (Fig. S5). The average coefficient from the individual members is smaller than ERA5, but the ensemble mean filters out some noise and amplifies the signal, leading to a coefficient closer to ERA5.

Next, the regression of the 200-hPa geopotential height anomalies onto the corresponding standardized SATI is analysed for ERA5 and SEAS5. Upper-level positive geopotential height anomalies (Fig. 5a) appear, which are responsible for the above-normal (warm) temperature anomalies over WSA. These upper-level geopotential height anomalies resemble the Circumglobal teleconnection (CGT) pattern during the early summer over the WSA region (Ding and Wang 2005). However, negative upper-level geopotential height anomalies (Fig. 5b) appear favouring the below-normal temperatures over WSA in the ENSO regressions (Fig. 5c). Moreover, the regression of predicted 200-hPa geopotential height anomalies onto the corresponding standardized SATI is also performed for each member in SEAS5. Figure 5d shows the mean of the 25 ensemble regression maps. Upper-level positive geopotential height anomalies (i.e., anticyclonic circulation anomalies) appear over north-west Pakistan. In contrast, negative anomalies appear for the ENSO (Niño3.4) regressions (Fig. 5e), favouring below normal SAT anomalies over WSA (Fig. 5f) during the positive ENSO (El Niño) phase, consistent with the ERA5. The opposite may happen in the cold ENSO phase, which is consistent with the findings of Rashid et al. (2022). Overall, the modelled ENSO teleconnection coincides well with the ERA5.

The Probability Distribution Function (PDF) of early summer seasonal SAT anomalies over the WSA in SEAS5 is assessed using KDE as shown in Fig. 6. Early summer SAT anomalies are binned into total (Climo) years (black), the La Niña (red), El Niño (blue) years category constraining them to the SEAS5 Niño3.4 (shown in dashed lines) as well as to the ERA5 Niño3.4 index (shown in solid lines). We noted both PDFs, i.e., constrained with SEAS5 and ERA5 Niño3.4 SST anomaly index, show a consistent pattern. A shift of SATI peak is noted towards the warm temperature anomalies during La Niña years, which may likely favour more frequent warm extremes, compared to El Niño (Fig. 6). Also, the probability of modulating hot extremes of about 2 °C temperature anomaly over the WSA region is about 15 times higher during La Niña, compared to the El Niño phase. Moreover, very hot extremes of about 2.5–3 °C anomaly are also more favourable during La Niña

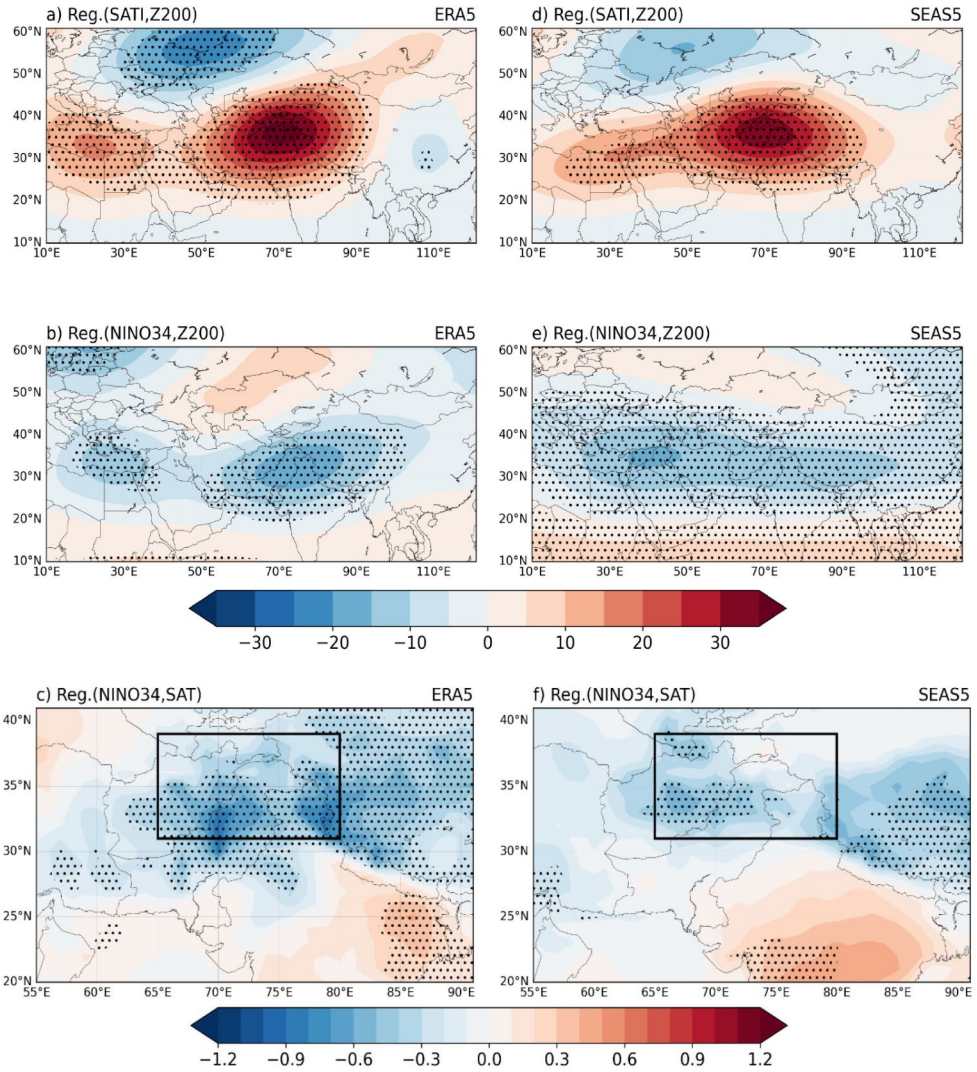

Fig. 5 **a-b**)ERA5 regression maps of 200-hPa geopotential height anomalies (Z200, Unit: m) onto standardized SATI, Niño3.4; and **c**) ERA5 regression of SAT onto the Niño3.4 index (Unit: °C), **d-f**) same as **a-c**) but for SEAS5, mean of the 25-ensemble members regression maps during early summer season for the period 1981–2022. Stippling represents the statistical significance at 95% confidence level

years. The broadening of the PDF around − 1.5 °C during El Niño shows that the warm ENSO phase more likely favours the amplitude of this temperature anomaly over the WSA region. Therefore, warm anomalies are more frequent during La Niña, and cold anomaly events are more frequent during El Niño years, consistent with Rashid et al. (2022). The SEAS5's ability to predict the SAT during El Niño and La Niña years will be discussed in Sect. 3.3.

Next, we analysed the spatial anomaly composites of temperature and the associated SSTs and 200-hPa geopotential height anomalies in the SEAS5 (Fig. 7) and ERA5 (Fig. S6) over the WSA region. The spatial composites are defined based on one-standard deviation of the SEAS5-based SATI over WSA, where values greater than and equal to one STD (i.e., ±0.94°C) are considered as positive ($SATI_p$) or warm years, and vice-versa for the negative ($SATI_n$) or cold years. The warm and cold years are selected from each ensemble member. It allows for a larger sample size for the extreme warm (160) and cold (167) years. Figure 7a shows the warm extremes ($SATI_p$) associated with the negative SST anomalies (Fig. 7c), which tend to favour upper-level positive geopotential height (Fig. 7b), while the opposite is noted for cold temperature extremes ($SATI_n$) over the WSA region (Fig. 7d-f). Similarly, Fig. S6 shows ERA5 warm (cold) extreme temperature composites based on one STD (Table S2). The SEAS5 spatial composites coincide well with the ERA5 (Fig. S6), suggesting SEAS5 is performing well in reproducing the essential features associated with extreme temperature conditions over the region. This validates SEAS5 utility for predicting temperature extremes over WSA, which will be discussed in Sect. 3.3.

3.3 Predictability of the early summer SAT over the West South Asia

Figure 8 shows the temporal evolution of the ERA5 SAT in comparison to the SEAS5 predicted temperatures. Each ensemble member is shown with a grey circle, while the

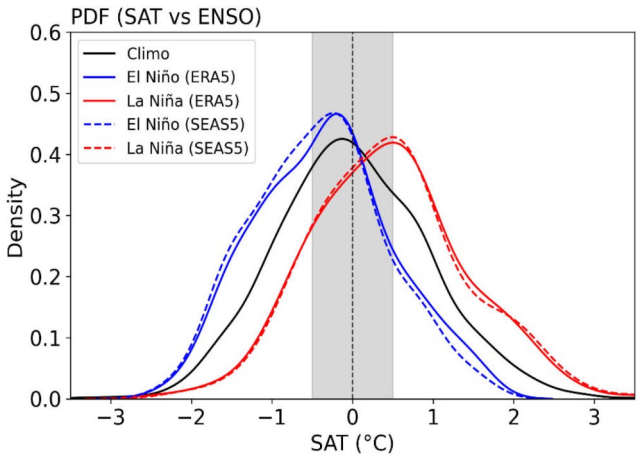

Fig. 6 Probability Distribution Function (PDF) of SAT anomalies over WSA region during La Niña (red), El Niño (blue) events and their climatological pdf (black) based on $25 \times 42 = 1050$ sample size during early summer for the period 1981–2022. The total numbers of La Niña and El Niño events in SEAS5 are 215 and 227 respectively based on the ERA5 Niño3.4 index (solid lines). The dashed line shows PDF based on concatenated SEAS5 Niño3.4 index, where total numbers of La Niña (red dashed line) and El Niño (blue dashed line) SAT events in SEAS5 are 250 and 225 respectively

ensemble mean SAT index is shown as the blue line. The SEAS5 ensemble mean tends to capture the SAT variability over the region quite well compared to the reanalysis (ERA5, green line), with some underestimation in the amplitude. Additionally, we also compared the different observational and reanalysis datasets with the SEAS5 predicted SAT over WSA (Fig. 8). All observational and reanalysis datasets (ERA5, NCEP, CRU, CPC, and MERRA-2) lie within the range of the SEAS5 ensemble spread. The actual skill of the SEAS5 temperature (r_{SAT}) with standard error for ERA5 is $r_{SAT} = 0.50 \pm 0.16$, while with NCEP is $r_{SAT} = 0.13 \pm 0.17$, CRU is $r_{SAT} = 0.44 \pm 0.12$, CPC is $r_{SAT} = 0.57 \pm 0.15$, and with MERRA-2 is $r_{SAT} = 0.43 \pm 0.15$. The uncertainty in temperature prediction skill varies among different observational and reanalyses. Notably, the SEAS5 shows higher temporal prediction skill against higher spatial resolution reanalysis and observational datasets (ERA5, CRU, CPC, and MERRA-2), whereas it exhibits lower skill when compared with the coarser resolution NCEP. Moreover, the lower SAT prediction skill of SEAS5 with NCEP over WSA could be related to the weaker ENSO-SAT teleconnections in NCEP compared to the other reanalysis and observational datasets, as shown in Fig. S7.

Next, we analysed the spatial pattern of the actual skill and the Potential Predictability (PP) of the SEAS5 SAT over the WSA region. Figure 9a shows that the actual skill of SEAS5 SAT is significant over the WSA region. The maximum actual skill (statistically significant at 95% confidence level; shown as stippling) appears over southern Uzbekistan, Afghanistan, north and northwestern Pakistan, northwest India, and western Nepal. Moreover, the spatial PP pattern of the SEAS5 SAT (Fig. 9b) is comparable to the actual skill, with slightly higher amplitude over the WSA region. The PP averaged over WSA is 0.48, comparable to the actual skill, and its spread noted with ERA5 (0.50 ± 0.16).

Moreover, the actual skill of SEAS5 SAT estimated against CRU, MERRA-2, and CPC (Fig. S8b, c,d) is comparable with the ERA5-based SEAS5 actual skill (Fig. 9a). Actual skill of SEAS5 SAT over WSA using NCEP shows a notable difference (Fig. S8a), which is consistent with the differences noted in its variability pattern (Fig. S1e). Furthermore, statistically significant actual skill and PP of SEAS5 SAT (Fig. 9a-b) are noted over the central and Southern Indian Peninsula regions. However, this discussion is beyond the scope of the present study, which could be discussed in future studies. Moreover, we also assessed the SEAS5 SAT prediction skill over the sub-regions, over Afghanistan, northwestern Pakistan, Uzbekistan, and northwest of India, as shown in Fig. 9. The highest PP and actual skill of SEAS5 SAT are noted over Afghanistan and northwestern Pakistan compared to the other sub-region within the WSA region.

To assess the spatial PP differences within WSA, we analysed the SEAS5 signal and noise variances. Figure 10a displays the signal variance of temperature, which is higher over the north and northwest of Pakistan and Afghanistan than Tajikistan, southern Uzbekistan, and northwest India and Nepal. A prominent noise variance is noted in the temperature over WSA (Fig. 10b), which is significantly large over the mountainous region, particularly over the foothills of the western HKH region. Higher noise in the mountainous region could be partially attributed to the complex topography, where SEAS5 might underestimate the remote forcing due to subtle differences in large-scale processes (Mehmood et al. 2022). SEAS5 deficiencies over high-altitude regions amplify these discrepancies.

Next, we estimated the SEAS5's ability to predict the SAT during El Niño and La Niña years over WSA, as shown in Fig. 11 (a-b). Figure 11b shows the PP for La Niña (0.42) is comparable to El Niño (0.41) years (Fig. 11a) averaged over the WSA domain. However, sub-regionally, the PP over northwest India is higher (statistically significant at 80% confidence level) in La Niña than El Niño, while over Uzbekistan, Afghanistan, and northwestern Pakistan, higher PP (statistically insignificant) is noted in La Niña than that of El Niño phase (Table 1). Overall, the signal and noise during La Niña (Fig. S9c-d) is about 41% (statistically significant at 95% confidence level) and 16% higher than El Niño over WSA (Fig. S9a-b). Moreover, sub-regionally, the signal is almost 67% higher over Uzbekistan, while over northwest India, it increases three times during La Niña compared to El Niño, contributing to the higher PP in the

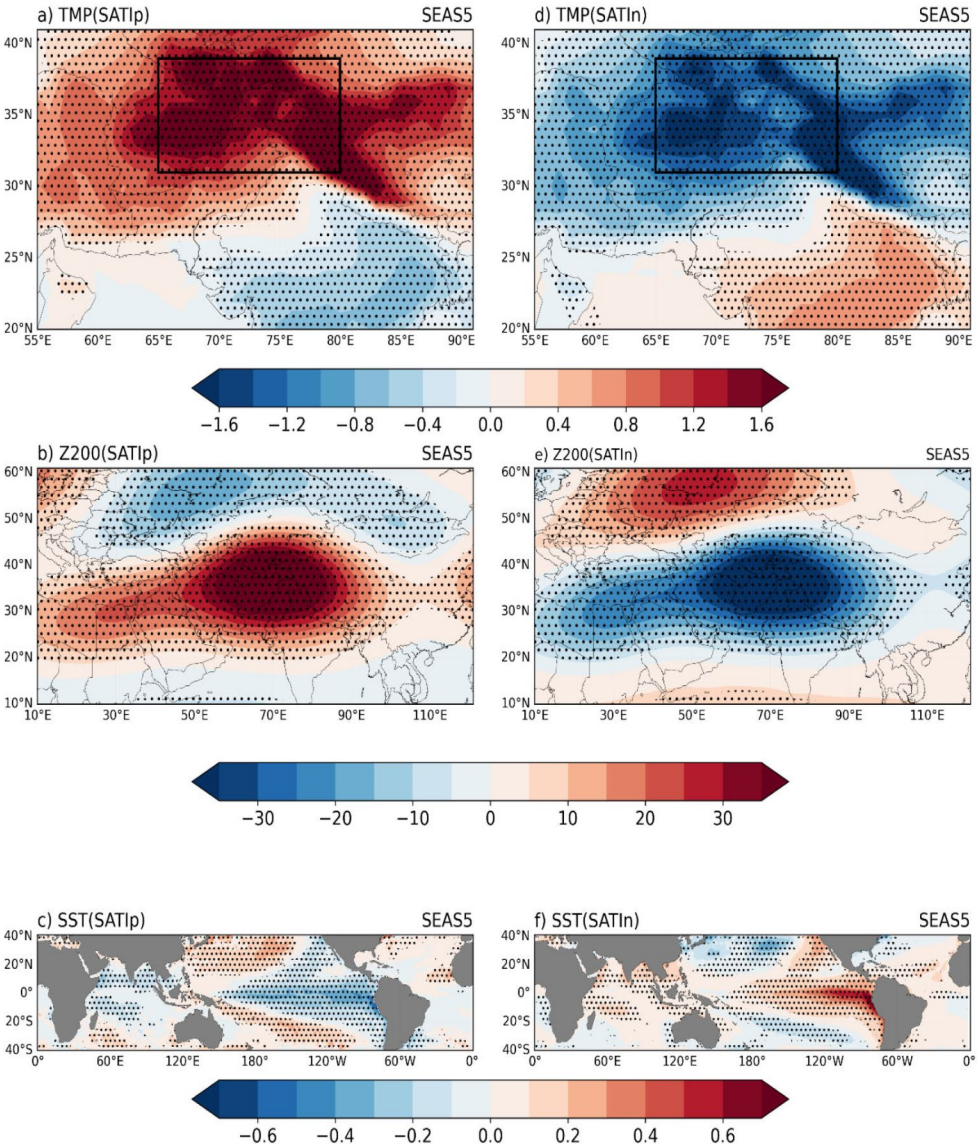

Fig. 7 **a-c**) SEAS5 SAT anomaly (Unit: °C) composite maps based on 25-ensemble members for the warm extreme years (referred as $SATI_p$), and the corresponding Z200 anomalies (Unit: m) and SST anomalies (Unit: °C) for the period 1981–2022; **d-f**) same as (**a-c**) but for cold temperature extreme composite anomalies (referred as $SATI_n$). Warm and Cold temperature extreme years are selected based on the ± 1 standard deviation of SEAS5 SATI over WSA region. Stippling represents the statistical significance at 95% confidence level

La Niña phase over these regions. We also assessed the PP for normal years, which is about 0.35 (statistically significant at the 95% confidence level) over WSA. The sources of the predictability in the non-ENSO years are yet to be known. Other tropical basins, such as the Indian (Abid et al. 2020; Mehmood et al. 2022) or Atlantic oceans (Ehsan et al. 2020), may play an important role, which could be explored in future studies.

4 Summary and discussion

In the present study, the SAT predictability is analysed over the WSA region during the early summer (May-June; MJ) season using the SEAS5 seasonal prediction system dataset based on April initial conditions (lead-1). The SAT variability and predictability are discussed from 1981 to 2022, after linearly removing global warming trends from observations, reanalyses, and SEAS5. ERA5 compares well with most of the datasets over WSA, where the strongest relationship is noted with CPC, CRU and MERRA-2, while a moderate relationship is noted with NCEP. SEAS5 predicts the SAT mean and variability reasonably well compared to the observed and reanalyses datasets during the early summer season, where the maximum SAT variability is noted over the WSA region.

ENSO teleconnections to the SAT over the WSA region are well represented in SEAS5 compared to the ERA5 reanalysis. A statistically significant negative relationship between ENSO and SAT over WSA is noted in ERA5 and SEAS5. It indicates the negative (or below normal) SST anomalies in the central-eastern equatorial Pacific region (i.e., La Niña) modulate the upper-level positive geopotential height anomalies, which are responsible for the

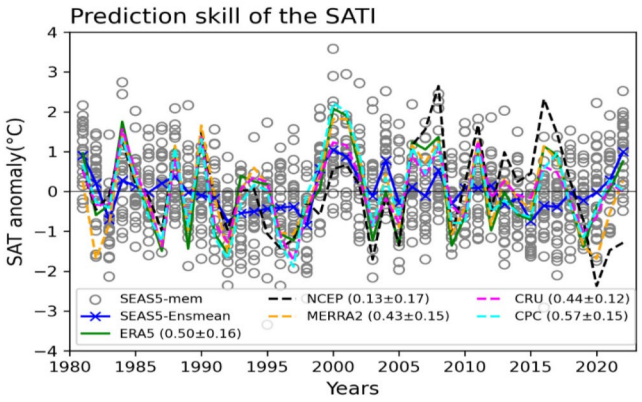

Fig. 8 Prediction skill of the SAT anomaly over the WSA region. Grey circles indicate SEAS5 each ensemble member SAT anomaly (Unit: °C) over WSA region, while blue line is the mean of the ensemble members, while green solid, black dashed, magenta dashed, orange dashed and cyan dashed are for ERA5, NCEP, MERRA-2, CRU and CPC respectively during early summer (May-June: MJ) season for the period 1981–2022. The prediction skill of the SAT anomalies during early summer season for SEAS5 with respect to ERA5 (green solid line) is 0.50 ± 0.16, NCEP (black dashed line) is 0.13 ± 0.17, MERRA-2 (orange dashed line) is 0.43 ± 0.15, CRU (magenta dashed line) is 0.44 ± 0.12 and CPC (cyan dashed line) is 0.57 ± 0.15

above-average temperatures or anomolous warm conditions over the WSA region. Conversely, the opposite happens during the warm phase of ENSO (i.e., El Niño). These findings are in accordance with those shown by Rashid et al. (2022). SEAS5 predicts the sensitivity of the SAT anomaly to the Niño3.4 SST anomalies reasonably well compared to ERA5, which shows the SAT over WSA is sensitive to the SST anomalies in the ENSO (Niño3.4) region.

Furthermore, we noted that La Niña tends to favour anomolous warm temperatures over the region, strongly increasing the probability of hot to very hot extremes compared to El Niño and total years. The SEAS5 skilfully represents the spatial circulation patterns favouring warm and cold temperature extremes over the region (Fig. 7), comparable to the ERA5 (Fig. S6). These findings about the ENSO-SAT relationship over WSA region differ from the eastern half of the South Asian region, where a positive ENSO-SAT relationship is noted (Zhou et al. 2019; Ehsan 2020). This shows the complexity of the South Asia region, where ENSO teleconnections show a contrasting result from the eastern to its western half.

The magnitude of the SEAS5 SAT prediction skill varies when measured against different observational and reanalysis datasets, where estimates against high-resolution datasets like ERA5, CRU, MERRA-2, and CPC show better skill, with a higher actual skill of 0.50 ± 0.16, 0.44 ± 0.12,

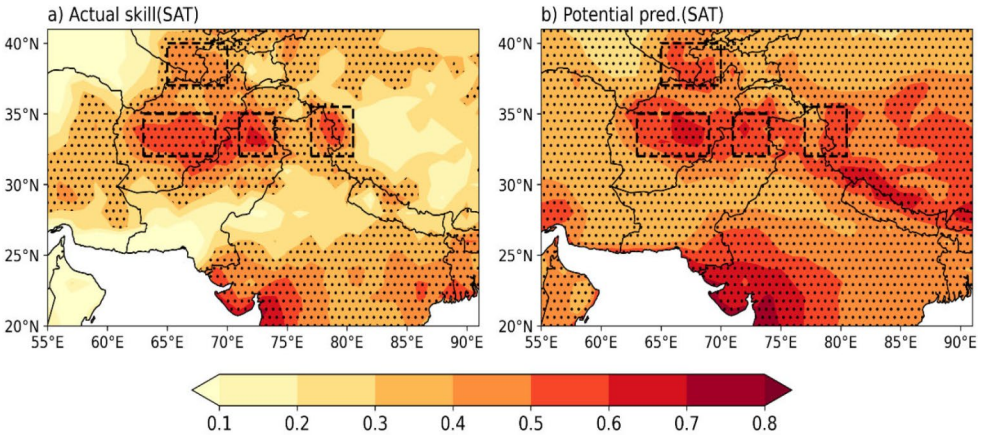

Fig. 9 **a**-**b**) Actual skill and Potential Predictability of SAT anomalies over WSA during early summer season for the period 1981–2022. Stippling represents the statistical significance at the 95% confidence level. Boxes with black dashed lines highlights the skill over northwestern Pakistan [71°E–74°E; 32°N–35°N], Afghanistan [63°E–69°E; 32°N–35°N], Uzbekistan [65°E–70°E; 37°N–40°N] and over northwest India [77°E-80.5°E; 32°N-35.5°N]

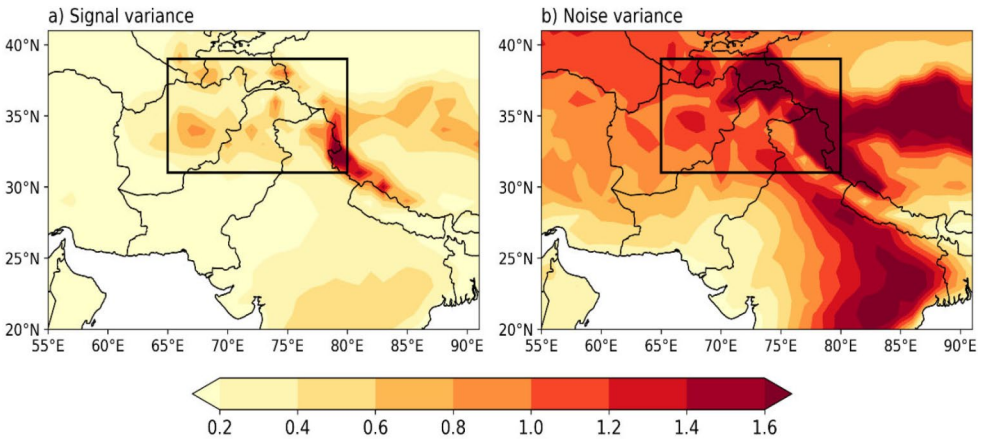

Fig. 10 (**a**) Signal variance; (**b**) Noise variance, (Unit: °C^2) of the SAT over WSA during early summer season for the period 1981–2022

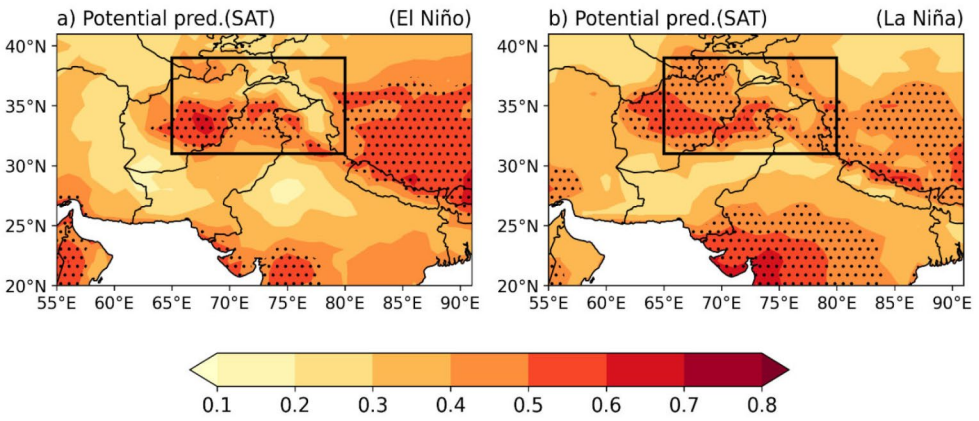

Fig. 11 Potential Predictability of the SAT over WSA region for (**a**) El Niño and (**b**) La Niña years during early summer season for the period 1981–2022. Stippling represents statistically significant values at 95% confidence level

Table 1 Potential predictability (PP) of the early summer season SAT for WSA and its sub-domains i.e., Northwestern Pakistan [71°E–74°E; 32°N–35°N], Afghanistan [63°E–69°E; 32°N–35°N], Uzbekistan [65°E–70°E; 37°N–40°N] and over Northwest India [77°E-80.5°E; 32°N-35.5°N] during El Niño and La Niña years for the period 1981–2022

Region	El Niño (PP)	La Niña (PP)
WSA	0.41	0.42
Afghanistan	0.51	0.49
Northwestern Pakistan	0.46	0.48
Uzbekistan	0.39	0.44
Northwest India	0.35	0.43

0.43 ± 0.15, and 0.57 ± 0.15, respectively. However, against the NCEP dataset, lower skill is noted (0.13 ± 0.17). This underscores the usefulness of higher spatial resolution datasets in regions with complex topography, such as WSA (Saini and Attada 2023). Also, it is pertinent to mention that ENSO teleconnections with SAT over WSA in CPC, CRU and MERRA-2 are comparable with ERA5, while weaker teleconnections are noted in NCEP, which could potentially be the reason for the weaker SEAS5 SAT prediction skill, assessed with NCEP.

Overall, SEAS5 demonstrates a PP of 0.48 of SAT over WSA, comparable to the actual skill estimated in most reanalysis and observational datasets except that of NCEP. Moreover, the SEAS5 SAT PP during the La Niña phase is comparable to El Niño years over WSA. A higher SAT PP is noted in all sub-regions within WSA during La Niña compared to El Niño years, but the difference in the two phases is only statistically significant at the 80% confidence level over northwest India, which is mainly contributed by the significant changes in the signal over this region. This shows that SEAS5 skilfully predicts anomolous temperature conditions over the sub-regions with higher confidence in predicting warm SAT extremes. It is pertinent to mention that ENSO explains about 18% of the total variance, which means there are likely other sources of predictability for the regional temperature that are currently unknown. These additional sources will be explored and discussed in future studies.

This study provides valuable insight into predicting anomolus temperature conditions on seasonal timescales over the WSA region during the early summer season. This information will be helpful for the regional stakeholders in strategic planning for the energy, agriculture, and water resources sector for the livelihood of a large population affected by temperature extremes on S2S timescales in the WSA region. There is a need for multi-model studies in the future to understand the diversity among the models in predicting the temperature extremes over the region on S2S timescales.

Supplementary Information The online version contains supplementary material available at https://doi.org/10.1007/s00382-024-07399-5.

Acknowledgements The lead author acknowledges the Pakistan Meteorological Department (PMD), Islamabad, Pakistan, for providing the necessary resources to conduct this study. The authors also acknowledge the support of the ESP at ICTP. M. Almazroui is supported by the Institutional Fund Projects grant number (IFPIP: 1194-155-144) and acknowledges the technical and financial support from the Ministry of Education and the Deanship of Scientific Research (DSR), King Abdulaziz University (KAU) Jeddah, Saudi Arabia. M. Ashfaq is supported by the U.S. Air Force Numerical Weather Modeling Program and National Climate-Computing Research Center, located within the National Center for Computational Sciences at the ORNL, and supported under a Strategic Partnership Project 2316-T849-08 between DOE and NOAA. M. A. Abid is supported by the UK Research and Innovation (UKRI) under the UK government's Horizon Europe project grant No. [101081460]. The authors thank two anonymous reviewers and editor for the constructive and insightful comments.

Author contributions The initial concept was discussed between I.U. Rashid and M. A. Abid, contributed equally in the preparation, analysis, writing, and reviewing the manuscript. M. Osman, F. Kucharski, M. Ashfaq, A. Weisheimer and José A. T-Alavez contributed to the discussion, writing, and revisions of the manuscript. M. Almazroui and M. Afzaal contributed to the discussions.

Data availability The Fifth generation European Re-Analysis (ERA5) reanalysis and the European Centre for Medium-Range Weather Forecasts fifth generation seasonal prediction system SEAS5 data used are

available through the https://cds.climate.copernicus.eu/. National Centre for Environmental Prediction (NCEP)/National Centre for Atmospheric Research (NCAR) data are available from https://psl.noaa.gov/data/gridded/data.ncep.reanalysis.html, the Climate Research Unit (CRU v4.04) data are available from https://crudata.uea.ac.uk/cru/data/hrg/cru_ts_4.04/, the Modern-Era Retrospective Analysis for Research and Applications, Version 2 (MERRA-2) data are available through https://daac.gsfc.nasa.gov/ and CPC Global Unified Temperature data provided by the NOAA PSL, Boulder, Colorado, USA, are available from their website at https://psl.noaa.gov/data/gridded/data.cpc.globaltemp.html. Topography data was obtained from following link (Dataset Overview | National Centers for Environmental Information (NCEI) (noaa.gov)). The computational codes are available on following link (https://github.com/madnanabid/westSouth_Temp-Predictability). Python, numpy (https://numpy.org/) and Matplotlib (https://matplotlib.org/) are also acknowledged.

Declarations

Competing interests The authors declare no financial and competing interest during the preparation of this manuscript.

References

Abid MA, Kang IS, Almazroui M, Kucharski F (2015) Contribution of synoptic transients to the potential predictability of PNA circulation anomalies: El niño versus la niña. J Clim 28:8347–8362. https://doi.org/10.1175/JCLI-D-14-00497.1

Abid MA, Kucharski F, Almazroui M, Kang IS (2016) Interannual rainfall variability and ECMWF-Sys4-based predictability over the Arabian Peninsula winter monsoon region. Q J R Meteorol Soc 142:233–242. https://doi.org/10.1002/qj.2648

Abid MA, Almazroui M, Kucharski F et al (2018) ENSO relationship to summer rainfall variability and its potential predictability over Arabian Peninsula region. npj Clim Atmos Sci 1:1. https://doi.org/10.1038/s41612-017-0003-7

Abid MA, Ashfaq M, Kucharski F et al (2020) Tropical Indian Ocean mediates ENSO Influence over Central Southwest Asia during the wet season. Geophys Res Lett 47:1–11. https://doi.org/10.1029/2020GL089308

Abid MA, Kucharski F, Molteni F, Almazroui M (2023) Predictability of Indian Ocean precipitation and its North Atlantic teleconnections during early winter. npj Clim Atmos Sci 6:17. https://doi.org/10.1038/s41612-023-00328-z

Almazroui M, Saeed S, Saeed F et al (2020) Projections of precipitation and temperature over the south Asian countries in CMIP6. Earth Syst Environ 4:297–320. https://doi.org/10.1007/s41748-020-00157-7

Almazroui M, Ehsan MA, Tippett MK et al (2022) Skill of the Saudi-KAU CGCM in forecasting ENSO and its comparison with NMME and C3S models. Earth Syst Environ 6:327–341. https://doi.org/10.1007/s41748-022-00311-3

Arshad M, Ma X, Yin J et al (2021) Performance evaluation of ERA-5, JRA-55, MERRA-2, and CFS-2 reanalysis datasets, over diverse climate regions of Pakistan. Weather Clim Extrem 33:100373. https://doi.org/10.1016/j.wace.2021.100373

Ashfaq M, Cavazos T, Reboita MS et al (2021) Robust late twenty-first century shift in the regional monsoons in RegCM-CORDEX simulations. Clim Dyn 57:1463–1488

Ashfaq M, Johnson N, Kucharski F et al (2023) The influence of natural variability on extreme monsoons in Pakistan. npj Clim Atmos Sci 6:148. https://doi.org/10.1038/s41612-023-00462-8

Attada R, Dasari HP, Chowdary JS et al (2018) Surface air temperature variability over the Arabian Peninsula and its links to circulation patterns. Int J Climatol. https://doi.org/10.1002/joc.5821

Campbell S, Remenyi TA, White CJ, Johnston FH (2018) Heatwave and health impact research: a global review. Heal Place 53:210–218. https://doi.org/10.1016/j.healthplace.2018.08.017

Chaturvedi RK, Kulkarni A, Karyakarte Y et al (2014) Glacial mass balance changes in the Karakoram and Himalaya based on CMIP5 multi-model climate projections. Clim Change 123:315–328. https://doi.org/10.1007/s10584-013-1052-5

Chelani AB, Rao PS (2013) Temporal variations in surface air temperature anomaly in urban cities of India. Meteorol Atmos Phys 121:215–221. https://doi.org/10.1007/s00703-013-0262-8

Chowdary JS, John N, Gnanaseelan C (2014) Interannual variability of surface air-temperature over India: impact of ENSO and Indian Ocean Sea surface temperature. Int J Climatol 34:416–429

Copernicus Climate Change Service (C3S) (2017) ERA5: fifth generation of ECMWF atmospheric reanalyses of the global climate. Copernicus Clim Chang Serv Clim Data Store (CDS), accessed 2018-05-04

Delsole T, Tippett MK, Shukla J (2011) A significant component of unforced multidecadal variability in the recent acceleration of global warming. J Clim. https://doi.org/10.1175/2010JCLI3659.1

Ding Q, Wang B (2005) Circumglobal teleconnection in the Northern Hemisphere summer. J Clim 18:3483–3505. https://doi.org/10.1175/JCLI3473.1

Eade R, Smith D, Scaife A et al (2014) Do seasonal-to-decadal climate predictions underestimate the predictability of the real world? Geophys Res Lett 41:5620–5628. https://doi.org/10.1002/2014GL061146

Ehsan MA (2020) Potential predictability and skill assessment of boreal summer surface air temperature of South Asia in the north American multimodel ensemble. Atmos Res 241:104974. https://doi.org/10.1016/j.atmosres.2020.104974

Ehsan MA, Kucharski F, Almazroui M et al (2019) Potential predictability of arabian peninsula summer surface air temperature in the north American multimodel ensemble. Clim Dyn. https://doi.org/10.1007/s00382-019-04784-3

Ehsan MA, Nicolì D, Kucharski F et al (2020) Atlantic Ocean influence on Middle East summer surface air temperature. npj Clim Atmos Sci 3:1–8. https://doi.org/10.1038/s41612-020-0109-1

Gelaro R, McCarty W, Suárez MJ et al (2017) The modern-era retrospective analysis for research and applications, version 2 (MERRA-2). J Clim 30:5419–5454

Hardiman SC, Dunstone NJ, Scaife AA et al (2022) Missing eddy feedback may explain weak signal-to-noise ratios in climate predictions. npj Clim Atmos Sci 5:57. https://doi.org/10.1038/s41612-022-00280-4

Harris I, Osborn TJ, Jones P, Lister D (2020) Version 4 of the CRU TS monthly high-resolution gridded multivariate climate dataset. Sci Data 7:109. https://doi.org/10.1038/s41597-020-0453-3

Hersbach H, Bell B, Berrisford P et al (2020) The ERA5 global reanalysis. Q J R Meteorol Soc 146:1999–2049. https://doi.org/10.1002/qj.3803

Hoell A, Hoerling M, Eischeid J, Barsugli J (2021) Preconditions for extreme wet winters over the contiguous United States. Weather Clim Extrem 33:100333. https://doi.org/10.1016/j.wace.2021.100333

Iqbal SW, Latif M, Ahmed R et al (2022) Performance evaluation and comparison of observed and reanalysis gridded precipitation datasets over Pakistan. Theor Appl Climatol 149:1093–1116. https://doi.org/10.1007/s00704-022-04100-w

Joshi MK, Rai A, Kulkarni A, Kucharski F (2020) Assessing changes in characteristics of hot extremes over India in a warming environment and their driving mechanisms. Sci Rep 10:1–14. https://doi.org/10.1038/s41598-020-59427-z

Kalnay E, Kanamitsu M, Kistler R et al (1996) The NCEP/NCAR 40-year reanalysis project. Bull Am Meteorol Soc 77:437–471

Kang D, Lee M-I (2019) ENSO influence on the dynamical seasonal prediction of the east Asian Winter Monsoon. Clim Dyn 53:7479–7495

Kang I-S, Shukla J (2006) Dynamic seasonal prediction and predictability of the monsoon. The Asian monsoon. Springer, pp 585–612

Kang IS, Lee JY, Park CK (2004) Potential predictability of summer mean precipitation in a dynamical seasonal prediction system with systematic error correction. J Clim 17:834–844. https://doi.org/10.1175/1520-0442(2004)017%3C0834:PPOSMP%3E2.0.CO;2

Kirtman BP, Min D, Infanti JM et al (2014) The north American multimodel ensemble: phase-1 seasonal-to-interannual prediction; phase-2 toward developing intraseasonal prediction. Bull Am Meteorol Soc 95:585–601

Kothawale DR, Munot AA, Kumar KK (2010) Surface air temperature variability over India during 1901–2007, and its association with enso. Clim Res. https://doi.org/10.3354/cr00857

Kucharski F, Abid MA (2017) Interannual variability of the Indian Monsoon and its link to ENSO. Oxf Res Encycl Clim Sci 1–24. https://doi.org/10.1093/acrefore/9780190228620.013.615

Kucharski F, Kang IS, Straus D, King MP (2010) Teleconnections in the atmosphere and oceans. Bull Am Meteorol Soc 91:381–383. https://doi.org/10.1175/2009BAMS2834.1

Kumar A, Peng P, Chen M (2014) Is there a relationship between potential and actual skill? Mon Weather Rev 142:2220–2227

Latif M, Syed FS (2016) Determination of summer monsoon onset and its related large-scale circulation characteristics over Pakistan. Theor Appl Climatol 125:509–520. https://doi.org/10.1007/s00704-015-1530-y

Lau KM, Kim MK, Kim KM (2006) Asian summer monsoon anomalies induced by aerosol direct forcing: the role of the Tibetan Plateau. Clim Dyn 26:855–864. https://doi.org/10.1007/S00382-006-0114-Z/FULLTEXT.HTML

Liu B, Wu G, Mao J, He J (2013) Genesis of the south Asian high and its impact on the asian summer monsoon onset. J Clim 26:2976–2991. https://doi.org/10.1175/JCLI-D-12-00286.1

Mannig B, Pollinger F, Gafurov A et al (2018) Impacts of climate change in Central Asia. Encyclopedia of the Anthropocene. Elsevier, pp 195–203

McPhaden MJ, Santoso A, Cai W (2020) El Niño Southern Oscillation in a changing climate. Wiley

Mehmood S, Ashfaq M, Kapnick S et al (2022) Dominant controls of cold-season precipitation variability over the high mountains of Asia. npj Clim Atmos Sci 5:65. https://doi.org/10.1038/s41612-022-00282-2

Molteni F, Stockdale TN, Vitart F (2015) Understanding and modelling extra-tropical teleconnections with the Indo-Pacific region during the northern winter. Clim Dyn 45:3119–3140

Nath S, Hauser M, Schumacher DL et al (2024) Representing natural climate variability in an event attribution context: Indo-Pakistani heatwave of 2022. Weather Clim Extrem 44:100671

NOAA N (2006) 2-minute gridded global relief data (etopo2) v2. Natl Geophys Data Center, NOAA Natl Centers Env Inf

Osman M, Vera CS (2017) Climate predictability and prediction skill on seasonal time scales over South America from CHFP models. Clim Dyn 49:2365–2383. https://doi.org/10.1007/s00382-016-3444-5

Osman M, Domeisen DIV, Robertson AW, Weisheimer A (2023) Subseasonal to decadal predictions in support of climate services. Clim Serv 100397

Palmer TN, Alessandri A, Andersen U et al (2004) Development of a European multimodel ensemble system for seasonal-to-interannual prediction (DEMETER). Bull Am Meteorol Soc 85:853–872. https://doi.org/10.1175/BAMS-85-6-853

Perkins SE (2015) A review on the scientific understanding of heatwaves-their measurement, driving mechanisms, and changes at the global scale. Atmos Res 164–165:242–267. https://doi.org/10.1016/j.atmosres.2015.05.014

Price G, Farhan A (2022) Building resilience to extreme weather in South Asia. https://www.cascades.eu/publication/building-resilience-to-extreme-weather-in-south-asia/

Pritchard HD (2019) Asia's shrinking glaciers protect large populations from drought stress. Nature 569:649–654. https://doi.org/10.1038/s41586-019-1240-1

Rai A, Saha SK, Pokhrel S et al (2015) Influence of preonset land atmospheric conditions on the Indian summer monsoon rainfall variability. J Geophys Res Atmos 120:4551–4563. https://doi.org/10.1002/2015JD023159

Rashid IU, Abid MA, Almazroui M et al (2022) Early summer surface air temperature variability over Pakistan and the role of El Niño–Southern Oscillation teleconnections. Int J Climatol 1–17. https://doi.org/10.1002/joc.7560

Saeed S, Müller WA, Hagemann S, Jacob D (2011) Circumglobal wave train and the summer monsoon over northwestern India and Pakistan: the explicit role of the surface heat low. Clim Dyn 37:1045–1060. https://doi.org/10.1007/s00382-010-0888-x

Saeed F, Hagemann S, Saeed S, Jacob D (2013) Influence of mid-latitude circulation on upper Indus basin precipitation: the explicit role of irrigation. Clim Dyn 40:21–38. https://doi.org/10.1007/s00382-012-1480-3

Saini R, Attada R (2023) Analysis of himalayan summer monsoon rainfall characteristics using Indian High-Resolution Regional Reanalysis. Int J Climatol

Scaife AA, Smith D (2018) A signal-to-noise paradox in climate science. npj Clim Atmos Sci 1:1–8. https://doi.org/10.1038/s41612-018-0038-4

Taschetto AS, Ummenhofer CC, Stuecker MF et al (2020) ENSO Atmospheric Teleconnections. In: El Niño southern oscillation in a changing climate. Wiley Online Library, pp 309–335

Thirumalai K, DInezio PN, Okumura Y, Deser C (2017) Extreme temperatures in Southeast Asia caused by El Ninõ and worsened by global warming. Nat Commun Doi. https://doi.org/10.1038/ncomms15531

Trenberth KE, Caron JM, Stepaniak DP, Worley S (2002) Evolution of El Niño–Southern Oscillation and global atmospheric surface temperatures. J Geophys Res Atmos 107:AAC–5

Vitart F, Robertson AW (2018) The sub-seasonal to seasonal prediction project (S2S) and the prediction of extreme events. npj Clim Atmos Sci 1:1–7

Vogel MM, Zscheischler J, Wartenburger R et al (2019) Concurrent 2018 hot extremes Across Northern Hemisphere due to Human-Induced Climate Change. Earth's Futur 7:692–703. https://doi.org/10.1029/2019EF001189

Wang B, Lee J-Y, Kang I-S et al (2009) Advance and prospectus of seasonal prediction: assessment of the APCC/CliPAS 14-model ensemble retrospective seasonal prediction (1980–2004). Clim Dyn 33:93–117

Wei W, Yang S (2021) Interaction between south asian high and Indian summer monsoon rainfall. Indian Summer Monsoon Var El Niño-Teleconnections Beyond 319–334. https://doi.org/10.1016/B978-0-12-822402-1.00016-8

Wilks DS (2006) Statistical Methods in the Atmospheric Sciences. 2nd ed. Int Geophys Ser, 91

Younas W, Tang Y (2013) PNA predictability at various time scales. J Clim 26:9090–9114. https://doi.org/10.1175/JCLI-D-12-00609.1

Zachariah M, AchutaRao TA K, et al (2022) Climate Change made devastating early heat in India and Pakistan 30 times more likely. World Weather Attrib 43

Zheng J, Li Y, Li J et al (2017) The relationship between Indo-Pacific Convection Oscillation and Summer Surface Air Temperature in Southern Asia. SOLA 13:199–204. https://doi.org/10.2151/sola.2017-036

Zhongming Z, Linong L, Wangqiang Z, Wei L (2021) Climate Change 2021. The Physical Science Basis

Zhou Z-Q, Zhang R, Xie S-P (2019) Interannual variability of summer surface air temperature over central India: implications for monsoon onset. J Clim 32:1693–1706